Digital Twins for Building Pseudo-Measurements

Marcel Zimmer, Maximilian Buechel, Florian Redder, Maximilian Mork, Thiemo Pesch, André Xhonneux, Dirk Müller, and Andrea Benigni, *Senior Member, IEEE*

***Abstract*— Building control architectures are strongly limited by the systematic lack of measurements at user-relevant locations. This article proposes a digital twin (DT) architecture grounded in correlated Gaussian processes (Corr-GPs) that provide information in the form of pseudo-measurements. Tested with thermal and CO_2 measurements collected from the field, close-to-person pseudo-measurements are provided based on the continuous input of remotely located measurement signals. In particular, detailed short-term as well as long-term results are provided for both temperature and CO_2 DTs. We show that the proposed approach is trainable on only a few days of measurements. This property makes the proposed approach especially useful in field applications, where alternative algorithms, such as, for example, neural network architectures, are not capable of dealing with small amounts of data. We demonstrate how to adjust the proposed approach to provide temperature and CO_2 DTs for the generation of pseudo-measurements. In the given framework, we show how to utilize the proposed DT to couple multiple reference sensors to provide close-to-person pseudo-measurements. By extending the Corr-GP approach to a nonzero prior mean formulation, we show how to reduce the included information by the reference sensors. More precisely, the extended approach can be defined as a DT with only a single reference sensor. This enables a reliable long-term application by avoiding the need for retraining caused by changing seasonalities within the signal characteristics. That is, we show that the DT trained in summer can be operated in winter.**

***Index Terms*— Air quality, digital twins (DTs), Gaussian processes, pseudo-measurements, thermal measurement.**

I. Introduction

PEOPLE spend approximately 60–70% of their time indoors [1], and this share is increasing even further [2]. As indoor air quality (IAQ) and thermal comfort (TC) directly relate to occupant well-being, productivity, and building energy consumption [3], [4], monitoring and control of IAQ and TC are essential elements of successful building operation.

Guidelines on TC have been implemented in the form of international standards, for example, through ISO 7730:2005 [5]. These standards are based on the calculation of a predicted mean vote (PMV), and a predicted predicted percentage of dissatisfied (PPD). Recent studies dealt with more adaptive approaches or even individual TC models that make use of numerous in-depth measurements such as skin temperature or heart rate measured via wearables [6]. Modern IoT-enabled technologies and sensor networks can significantly improve occupant comfort and outperform classical approaches [6]. However, they also require a high number of additional sensors, a sophisticated IoT setup [7], and a high level of data protection [8], [9].

Two prominent and widespread indicators for building indoor comfort are the temperature [10] and the CO_2 level representing air quality [11]. Both quantities are commonly measured once per building space, for example, in the form of a sensor integrated into a room control panel. Based on the obtained air temperature and a user-defined temperature setpoint, either the buildings' central heating or a room-individual heating appliance, for example, a radiator, is operated to establish TC [12]. In this typical scenario, the control performance, and thus the TC, is strongly affected by sensor placement and accuracy. Nowadays, the trend is moving toward multiple stationary sensors per room at different locations, even in existing buildings [12]. It would therefore be of great benefit to be able to use these measurements to predict individual, close-to-person temperature profiles and thereby unlock comfort improvements and energy-saving potentials in building operation. Both standard (e.g., P/PI/PID) and advanced control concepts, for example, model predictive controllers (MPCs) could thus be upgraded to provide comfort specifically to the occupied zone. At the same time, additional (personal) sensor hardware would be avoided, which otherwise would result in additional financial effort and, as being located in the occupied zone, could constitute a disturbance to the occupants.

In this context, digital twins (DTs) have been applied [13]. DTs have gained widespread attention across different engineering disciplines [14] and applications spread from the temperature distribution of power equipment [15] and power electronics [16], to DT-driven measurements in robotics [17] and real-time monitoring of electric distribution grids [18]. Reviewed in [13], DTs are applied for TC and energy efficiency in buildings. In this field, applications range from specific quantities, such as energy saving by lighting [19], to heterogeneous data approaches [20]. However, so far, dedicated algorithms applied as in our proposed conceptual

Received 28 August 2024; revised 11 November 2024; accepted 2 December 2024. Date of publication 13 January 2025; date of current version 27 January 2025. This work was supported by the Helmholtz School for Data Science in Life, Earth and Energy (HDS-LEE). The Associate Editor coordinating the review process was Dr. Yang Song. *(Corresponding author: Marcel Zimmer.)*

Marcel Zimmer, Maximilian Buechel, Florian Redder, Maximilian Mork, Thiemo Pesch, and André Xhonneux are with the Institute of Climate and Energy Systems (ICE-1), Forschungszentrum Jülich, 52425 Jülich, Germany (e-mail: m.zimmer@fz-juelich.de; m.buechel@fz-juelich.de; f.redder@fz-juelich.de; m.mork@fz-juelich.de; t.pesch@fz-juelich.de; a.xhonneux@fz-juelich.de).

Dirk Müller is with the Institute of Climate and Energy Systems (ICE-1), Forschungszentrum Jülich, 52425 Jülich, Germany, also with JARA-Energy, 52425 Jülich, Germany, and also with the Institute for Energy Efficient Buildings and Indoor Climate, RWTH Aachen University, 52074 Aachen, Germany (e-mail: dmueller@eonerc.rwth-aachen.de).

Andrea Benigni is with the Institute of Climate and Energy Systems (ICE-1), Forschungszentrum Jülich, 52425 Jülich, Germany, also with JARA-Energy, 52425 Jülich, Germany, and also with Faculty of Mechanical Engineering, RWTH Aachen University, 52056 Aachen, Germany (e-mail: a.benigni@fz-juelich.de).

Digital Object Identifier 10.1109/TIM.2025.3527590

structure have not been used to provide indoor close-to-person temperature or CO_2 pseudo-measurements [13]. Pseudo-measurements have been considered in the domain of distribution grids [18], uncertainty quantification of power system state estimation [21], as well as for estimation of GPS outages [22].

In this work, which is an extension of [23], we propose the concept of DTs for indoor temperature and CO_2 pseudo-measurements and propose a realization by correlated Gaussian processes (Corr-GPs). First, we provide temperature and CO_2 pseudo-measurements for a user-relevant position based on two permanently installed sensors, called reference measurements hereafter, in a real-life office building. In addition to the reference measurements installed at standard locations, an additional measurement is collected at a user-relevant position. Based on the three measurements, a correlated Gaussian process is trained. Then, we show how to define a nonzero prior mean function in the context of thermal and CO_2 DTs for pseudo-measurement generation. This accounts for training the proposed approach by deviations from typical patterns instead of the signals themselves. By that, not only a reliable long-term application can be archived without the need for retraining the DT but also a single reference sensor suffices as input. We give a twofold evaluation of the proposed approach with respect to a trivial algorithm (TRIV) as well as a standard time-series vector autoregression moving average model (VARMA) [24]. First, the performance of the proposed approach is evaluated and compared to the given alternative algorithms with respect to the consecutive 14 days after the training period. Second, a seven-month long-term analysis is provided. We show that the proposed multiinput approach outperforms the given alternatives, due to its ability to determine inherent correlations across different measurements. The provided results indicate the superior ability of Corr-GPs to incorporate multiple signals, providing an algorithmic solution for multisensor-equipped rooms and buildings. Moreover, we show that the single-input Corr-GP can be reliably utilized in long-term applications.

This article is organized as follows. In Section II, the theoretical background is given. In Section III, we present the proposed method. In Section IV, the case study is described. The results are given in Section V. We conclude with Section VI.

II. Theoretical Background

A. Gaussian Processes

A Gaussian process is a collection of random variables, any finite number of which have a joint Gaussian distribution [25]. For the training set $(\mathcal{X}, \mathcal{Y})$ and the test set $\mathcal{X}^*$, this formally translates to the following equations. Let $\mathcal{X}$ be a compact subset of $\mathbb{R}^n$. We call $\mu_{\text{prior}} : \mathcal{X} \to \mathbb{R}$ a prior mean function and the positive semi-definite function $\kappa : \mathcal{X} \times \mathcal{X}' \to \mathbb{R}$ a kernel or kernel matrix with

$$K(\mathcal{X}, \mathcal{X}')_{\text{kl}} := (\kappa(x_k, x_l)) \quad \forall x_k \in \mathcal{X}\ \forall x_l \in \mathcal{X}'. \tag{1}$$

Adding $I\sigma_n$, where I denotes the identity matrix and $\sigma_n \in \mathbb{R}$ incorporates noise into the kernel, that is,

$$K_n(\mathcal{X}, \mathcal{X}) = K(\mathcal{X}, \mathcal{X}) + I\sigma_n. \tag{2}$$

The posterior mean μ_{post}, that is, the predictions, and the posterior covariance function Σ_{post}, are computed by

$$\mu_{\text{post}} = \mu_{\text{prior}}(\mathcal{X}^*) + K(\mathcal{X}^*, \mathcal{X})K_n(\mathcal{X}, \mathcal{X})^{-1}(\mathcal{Y} - \mu_{\text{prior}}(\mathcal{X})) \tag{3}$$

and

$$\Sigma_{\text{post}} = K(\mathcal{X}^*, \mathcal{X}^*) - K(\mathcal{X}^*, \mathcal{X})K_n(\mathcal{X}, \mathcal{X})^{-1}K(\mathcal{X}, \mathcal{X}^*). \tag{4}$$

The GP is trained by specifying a set of hyperparameters defining κ by minimizing the negative log marginal likelihood

$$\text{nlml} = \frac{1}{2}(\mathcal{Y} - \mu_{\text{prior}}(\mathcal{X}))^T K_n(\mathcal{X}, \mathcal{X})^{-1}(\mathcal{Y} - \mu_{\text{prior}}(\mathcal{X})) + \frac{1}{2}\ln|K_n(\mathcal{X}, \mathcal{X})| + \frac{N}{2}\ln(2\pi), \tag{5}$$

where N denotes the number of training data points. To specify the corresponding model, we write $\mathcal{GP}(\mu_{\text{prior}}, K(\mathcal{X}, \mathcal{X}'))$ throughout the article.

B. Alternative Algorithms

Contrary to GPs, the alternative models, called TRIV and VARMA as defined below, rely on equidistant time steps considering only the latest change-of-value (COV) measurement per time step.

The TRIV-model providing pseudo-measurements S_{DT} with respect to one $M = \{1\}$ or two $M = \{1, 2\}$ reference measurements $T_m, m \in M$ and is defined as

$$\text{TRIV} = \frac{1}{2}\sum_{m=1}^{M}\left(S_{mj}^{\text{offset}} + S_{mj}\right), \tag{6}$$

with $S_{mj}^{\text{offset}} = (1/i)\sum_i (T_{mji} - T_{\text{DT}_{ji}})$, where i is indexing training days and j indexing time steps during a day.

The VARMA-model for one $\vec{S} = (S_1, S_{\text{DT}})^T$ and two $\vec{S} = (S_1, S_2, S_{\text{DT}})^T$ reference measurements, respectively, reads

$$\text{VARMA} = \nu(t_j) + \text{AR}(p) + \vec{\epsilon}_j + \text{MA}(q), \tag{7}$$

with autoregression $\text{AR}(p) = A_1\vec{S}_{m_{j-1}} + \cdots + A_p\vec{S}_{m_{j-p}}$, moving average $\text{MA}(q) = M_1\vec{\epsilon}_{j-1} + \cdots + M_q\vec{\epsilon}_{j-q}$, Gaussian white noise $\vec{\epsilon}_j \sim N(0, \vec{\sigma}^2)$, and a linear trend $\nu(t_j) = \vec{a} + \vec{b}t_j$ for 2 or 3-D square matrices $A_1, \ldots, A_p, M_1, \ldots, M_q$ and vectors $\vec{a}, \vec{b} \in \mathbb{R}^3$ or $\mathbb{R}^2$, respectively. A least-squares algorithm is used for training. In the given case study, we have $p = q = 4$. Stationarity is achieved by subtracting the average daily profile, analogous to the trivial approach.

III. Proposed Approach

A. DT For Pseudo-Measurements

The proposed concept of a DT for pseudo-measurements is presented in Fig. 1. In the upper panel of Fig. 1, the training phase of the model is shown. For a certain period, all collected signals are used as training data for the DT. In the execution phase, depicted in the lower panel of Fig. 1, the reference signals are continuously included in the model, while the signal of interest is predicted at times t^* of interest. It should be noted, that there are two notions of inputs and outputs, visualized in Fig. 1. Reference signals are continuously included (DT input) while the signal of interest is predicted (DT output). For further

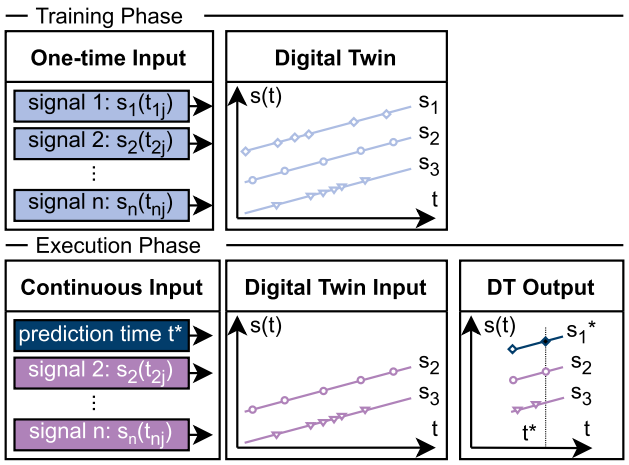

Fig. 1. Proposed DT concept.

clarify, we write $\mathrm{DT}_{\text{input}}^{\text{output}}$ throughout the article. However, inside the digital-twin realization by a Corr-GP described next, the reference signals as well as the predictions are both outputs of the multioutput GP (GP output), as functions of time (GP input).

On an intraday basis, every new reference measurement is continuously included in the DT to update the adaptive model in a rolling horizon fashion. As visualized in Fig. 2, for every new day N, the data of the previous day $N-1$ is deleted on a daily basis. The proposed approach is only updated with the data from the day on which the pseudo-measurements should be provided. The DT runs between 8:00 am (t_{start}) and 7:00 pm (t_{end}). In addition, an initialization phase, labeled as init in Fig. 2, is used, where before the operational period, reference measurements are included.

B. Correlation-Based Gaussian Processes for DTs

Certainly, correlations between differently located measurements of temperature signal $T(t), t \in \mathcal{T}$, as well as CO_2 signals, within a room are given. The key mathematical operation reflecting this correlation property is given by the tensor product, denoted by $\otimes$, yielding GP models with multiple outputs [25], [26]. This construction of a separable kernel is a composition of a kernel describing an individual signal's characteristics and a cross-correlation kernel. Thus, the proposed structure accounts for qualitative similarities across neighboring sensor measurements by construction. We refer to such models within the class of multioutput GPs as Corr-GP [26].

In terms of matrices, the tensor product is given by the Kronecker product, also denoted by $\otimes$. In particular, for a kernel matrix $K(\mathcal{T}, \mathcal{T}')$ and a symmetric positive semi-definite $d \times d$-matrix $B^{[d]}$, we have a d-dimensional model by

$$B^{[d]} \otimes K(\mathcal{T}, \mathcal{T}') = \begin{pmatrix} b_{1,1}K(\mathcal{T}, \mathcal{T}') & \dots & b_{1,d}K(\mathcal{T}, \mathcal{T}') \\ \vdots & \ddots & \vdots \\ b_{d,1}K(\mathcal{T}, \mathcal{T}') & \dots & b_{d,d}K(\mathcal{T}, \mathcal{T}') \end{pmatrix}. \quad (8)$$

The dimension d of the coregionalization matrix, $B^{[d]}$, corresponds to the number of coupled signals. A self-contribution

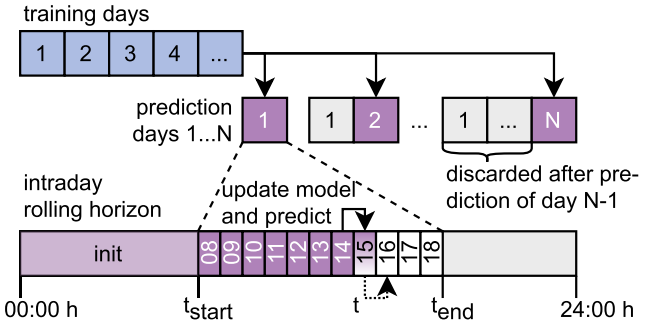

Fig. 2. Intraday rolling horizon for DT pseudo-measurement.

to the model of the individual measurements is given on the diagonal of (8) while off-diagonal elements describe correlations across measurements provided by different sensors. Thus, the trainable hyperparameters $\{b_{1,1}, \dots, b_{d,d}\}$ can be seen as weights of individual contributions from the respective measurements.

With this at hand, we may define a class of models, called the linear coregionalization model (LCM), given by

$$K_{\text{LCM}}(\mathcal{T}, \mathcal{T}') = \sum_q B_q^{[d]} \otimes K_{\text{basis},q}(\mathcal{T}, \mathcal{T}'), \quad (9)$$

where q corresponds to the number of considered signals in the given application.

The needed dataset defining the training period is a result of this definition. The single-signals hyperparameters describing intraday characteristics can be determined by a single day of data. To determine the correlation hyperparameters $\{b_{1,1}, \dots, b_{d,d}\}$ data reflecting the correlations must be provided. For the given case study, the minimal training period reflecting this is given by a dataset of five days.

For the given approach, hyperparameters σ_n present in (2) reflect the input sensor noise level. As part of the GP, these hyperparameters can be trained on the provided dataset. Thus, the sensor accuracy does not have to be individually considered but is determined from the training dataset.

1) Temperature Profiles: Room-temperature profiles do not vary extensively during the day. This type of smooth variation can be captured by the rational quadratic kernel RQ, given by

$$K_{\text{RQ}}(t, t') = \left(1 + \frac{|t - t'|}{2\alpha l^2}\right)^{-\alpha}, \quad (10)$$

with $\alpha, l \in \mathbb{R}^+$. It should be noted that the prediction scheme described in Fig. 2 is a consequence of this choice as (10) is defined by an Euclidean distance. An operation like this implies the model staying in the vicinity of the training set. In addition, a scaling by a constant factor is applied to ensure stable scaling during operation.

2) CO_2 Profiles: Contrary to temperature profiles, CO_2 profiles tend to vary more rapidly. Thus, a kernel with less amount of smoothness, that is, a Matérn kernel

$$K_{\text{M}^{5/2}}(t, t') = \left(1 + \frac{\sqrt{5}|t - t'|}{l} + \frac{5(t - t')^2}{3l^2}\right) \cdot \exp\left(\frac{-\sqrt{5}|t - t'|}{l}\right), \quad (11)$$

with length-scale hyperparameter $l \in \mathbb{R}^+$ has to be selected.

C. Nonzero Mean Functions for DTs

Within general Gaussian process applications, a nonzero mean function might be used to incorporate prior knowledge about the functions to be described [25]. This might be realized by a parametric model of the function if detailed knowledge about the signal characteristics is available. In the given data-driven application, an analytic function cannot be given as temperature and CO_2 signal characteristics are determined by nonmeasured quantities like occupancy within the room or solar radiation. However, it turns out to be sufficient to select the trivial approach (6) with $S = 1$ as a prior mean function, that is,

$$\mu_{\text{prior}}(t) = \text{TRIV}. \tag{12}$$

Contrary to the zero-mean approach previously discussed, this type of model is trained on the correlation between deviation from the trivial expectation instead of the correlation across signals themselves. As will be experimentally verified in Section V, this allows to rely on only a single reference sensor as input for the DT. Moreover, this enables a long-term application without the need for dedicated retraining strategies. This is because external changes, like for example seasonality, are affecting all measurements as well as pseudo-measurements present likewise. Thus, the proposed model trained on correlations of deviations is not significantly affected by changing seasons.

It should be noted that in the case of a single-input reference signal, the multioutput kernel (9) reduces to

$$K_{\text{ICM}}(\mathcal{T}, \mathcal{T}') = B^{[2]} \otimes K_{\text{basis}}(\mathcal{T}, \mathcal{T}'), \tag{13}$$

called the intrinsic coregionalization model (ICM).

IV. Case Study

The validity of the proposed approach is evaluated in a case study based on data collected from a real-life office building. The building is part of a set of facilities of Forschungszentrum Jülich GmbH that were equipped with additional measurement and automation capabilities in the scope of the living lab energy campus (LLEC) initiative [12]. These serve as a test-bed for the application and evaluation of advanced building monitoring and control strategies [27].

For this case study, we select a multipurpose room that is used as both a student laboratory and meeting room, displayed in Fig. 3. The room is furnished with multiple workstations and has three glass facades oriented in SE, SW, and NW directions. All three facades can be fully shaded through manual blinds operation via a wall-mounted control panel [human machine interface (HMI)].

There are three air-temperature signals available for the selected room: 1) one permanent measurement integrated into the HMI, which is located next to the main entrance door at a height of 1.60 m providing data on change of value (COV) with an accuracy of ±0.5 K and bound to a resolution of 0.1 K; 2) one additional permanent measurement as part of a ceiling-mounted presence-multisensor (PM) providing data on COV with an accuracy of ±0.2 K and bound to a resolution of 0.1 K; and 3) a temporary measurement via an on-desk personal IAQ sensor providing data every 5–15 min (depending on the dynamics of the measured values) with an accuracy of ±0.5 K and bound to a resolution of 0.2 K.

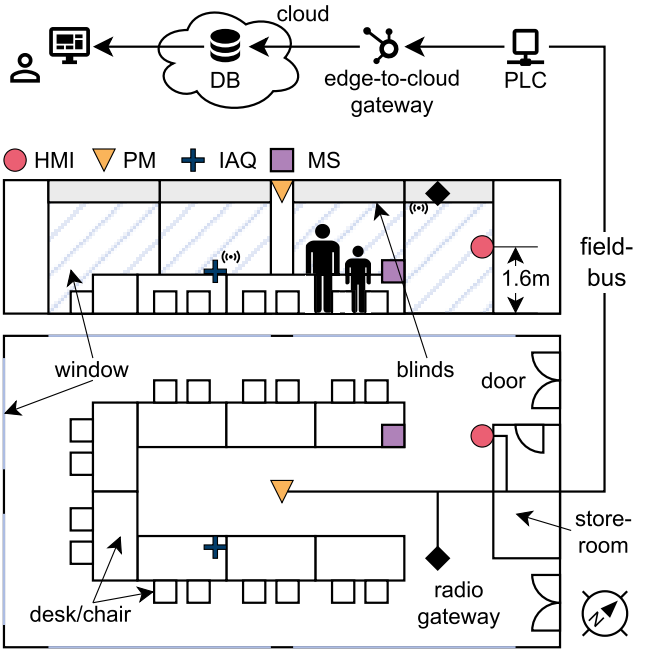

Fig. 3. Measurement setup for obtaining temperature data at different locations inside the test room.

The temperature measurement from the HMI constitutes a TC parameter that is quite commonly available in modern buildings nowadays [12]. This is due to the use of the room air temperature information to control the heating system based on a temperature set-point provided by the occupants. As the HMI is anyway required to obtain these set points, integrating a temperature measurement represents the industry's best practice. However, the location of the HMI does not allow for a measurement close to the occupants, which leads to a mismatch between the measurable and the occupant-experienced TC. An increasingly common second sensor at a different location, in this case, the ceiling-mounted PM sensor, can be used to better approximate the real room air temperature. The third temperature signal from the desk-mounted IAQ sensor is the best approximation of the real temperature experienced by a person in the room.

The on-desk sensor (IAQ) and the PM not only measure the air temperature but also the CO_2 concentration. In addition to these two CO_2 signals, a third one is available through a sensor that is also mounted on a desk [multi-sensor (MS)] but at a comparably remote position in a presumably better-ventilated part of the room. We choose this spot to achieve a measurement comparable to that of a conventional wall-mounted sensor while still being able to capture the important dynamics inside the occupied area of the room. Regarding the sensors' properties in terms of CO_2, both IAQ and MS have an accuracy of ±125 ppm. The accuracy of the PM sensor is slightly higher in comparison at ±90 ppm. All three devices have a resolution of 10 ppm and report new CO_2 values with the same sampling

TABLE I
SUMMARY OF IMPORTANT SPECIFICATIONS OF THE DEVICES USED IN THE CASE STUDY

Device	Manufacturer	Model	Protocol	Quantities	Accuracy	Resolution	Range	Sampling
IAQ, MS	Pressac Communications	60_CO2_SLR_-TMP_HUM_868	EnOcean[1] (A5-09-04)	Temperature	$\pm 0.5\,\mathrm{K}$	$0.2\,\mathrm{K}$	0–$51\,^{\circ}\mathrm{C}$	5–15 min[2]
				CO_2	$\pm 125\,\mathrm{ppm}$	$10\,\mathrm{ppm}$	0–$2555\,\mathrm{ppm}$	
HMI	MDT Technologies	BE-GT2TW.02	KNX-TP	Temperature	$\pm 0.5\,\mathrm{K}$	$0.1\,\mathrm{K}$	0–$40\,^{\circ}\mathrm{C}$	on COV
PM	STEINEL	True Presence Multisensor KNX	KNX-TP	Temperature	$\pm 0.2\,\mathrm{K}$	$0.1\,\mathrm{K}$	0–$40\,^{\circ}\mathrm{C}$	on COV
				CO_2	$\pm 90\,\mathrm{ppm}$	$10\,\mathrm{ppm}$	400–$10\,000\,\mathrm{ppm}$	
PLC	Beckhoff Automation	CX5130	ADS	n/a	n/a	n/a	n/a	10 ms[3]

[1] The EnOcean Equipment Profile (EEP) is provided here as it defines not only the payload of the telegram but also the resolution of the transmitted data.
[2] The sampling rate depends on the dynamics of the measured values; the higher the fluctuations, the higher the sampling rate and vice versa.
[3] The sampling rate, here, represents the cycle time of the PLC.

rate as for the temperature observations. We summarize sensor specifications in Table I.

Measurements from the four sensors are collected using a cloud-based infrastructure [12], [28]. Each sensor is connected to a programmable logic controller (PLC) via a KNX field-bus network. The IAQ and MS sensors are wireless sensors that use the radio-based EnOcean protocol and connect to the KNX bus through a dedicated, bidirectional EnOcean-to-KNX gateway. The other two sensors (HMI and PM) are directly connected to the KNX bus. The collected device data is transferred from the PLC into a time-series database. This is done via a data transfer script, which fetches the data from the PLC using the ADS protocol. The fetching mechanism is driven by changes in the data on the PLC to achieve low latencies in data transmission. Finally, the sensor data is retrieved from the database, which is deployed in a cloud environment, using structured query language (SQL) statements.

The dataset used in this case study contains five full days of measurements for training, 14 days for the short-term, and seven months for the long-term evaluation. Temperature and CO_2 data from the four sensors HMI, PM, IAQ, and MS, with varying temporal resolutions ranging from seconds to hours, was obtained from 01 June to 31 December 2023.

V. RESULTS

The evaluation of the overall performance and the comparison to alternative algorithms is given with respect to the normalized root mean squared error (NRMSE), that is,

$$\mathrm{NRMSE}(S_{\mathrm{DT}}, S_{\mathrm{IAQ}}) = \frac{1}{\bar{S}_{\mathrm{IAQ}}}\sqrt{\frac{1}{N}\sum_{j=1}^{N}(S_{\mathrm{IAQ},j} - S_{\mathrm{DT},j})^2}, \quad (14)$$

with N true measurements S_{IAQ} and, correspondingly, predicted pseudo-measurements S_{DT}. $\bar{S}_{\mathrm{IAQ}}$ denotes the arithmetic signals average for this specific period. It should be noted that (14) provides a relative error per day. That is, j runs over N time instances for each individual day. Long-term evaluations are performed per month, where the arithmetic mean over daily relative errors are computed.

A. Multiinput Temperature DTs

Developed in Section III, the proposed Corr-$\mathrm{GP}^{\mathrm{IAQ}}_{\mathrm{HMI,PM}}$ is calculated according to Figs. 1 and 2 and is defined by (9) with $q = 2$ using (10), that is,

$$\mathrm{DT}^{\mathrm{IAQ}}_{\mathrm{HMI,PM}} = \mathcal{GP}\left(0, \sum_{q=\mathrm{HMI,PM}} B_q^{[3]} \otimes K_{\mathrm{RQ}}(\mathcal{T}, \mathcal{T}')\right). \quad (15)$$

1) Detailed Short-Term Analysis: In Fig. 4, the comparison of the proposed Corr-$\mathrm{GP}^{\mathrm{IAQ}}_{\mathrm{HMI,PM}}$ DT (blue) with the $\mathrm{TRIV}^{\mathrm{IAQ}}_{\mathrm{HMI,PM}}$ (orange) and $\mathrm{VARMA}^{\mathrm{IAQ}}_{\mathrm{HMI,PM}}$ (green) model evaluated by NRMSE [%] per day can be seen. The proposed approach outperforms the given alternatives, for the entire evaluation set except for day 7. This can be explained via a distinct correlation on that specific day, which can be quantified, for example, in terms of the Pearson correlation coefficient [29], given by

$$r_i^{\mathrm{IAQ}} = \frac{\sum_j (T_{i_j} - \bar{T}_i)(T_{\mathrm{IAQ}_j} - \bar{T}_{\mathrm{IAQ}})}{\sqrt{\sum_j (T_{i_j} - \bar{T}_i)^2}\sqrt{\sum_j (T_{\mathrm{IAQ}_j} - \bar{T}_{\mathrm{IAQ}})^2}}, \quad (16)$$

where $T_i \in \{T_{\mathrm{HMI}}, T_{\mathrm{PM}}\}$, j runs over times instances during a day and bars denote the arithmetic average. The calculated r_i^{IAQ} for the given time-series are displayed in Fig. 5(a). It can be seen that on day seven, a lack of correlation between the IAQ measurements and both the HMI and PM measurements is evident. In line with the given theoretical construction of the Corr-GP in terms of separable kernels in Section III-B, this result indicates a strong connection between the proposed Corr-GP approach and the level of correlation across the considered signals. Considering Fig. 5(b), this can be explained by a transition in the shading position on day 7 at 10:24 am, in which the previously fully opened blinds are completely closed by the user. Solar radiation that is transmitted into the room heats up the room surfaces and, if hitting a sensor, results in an increased measured temperature. Hence, changes in shading intensity affect the correlation between the temperature sensors. For a prospective field application of Corr-GPs, this relation has to be investigated in detail and corresponding dedicated strategies have to be developed. As an example, the information on the blinds could be included in the DT.

2) Long-Term Statistical Analysis: As an additional test of the proposed approach, we give a long-term evaluation. The daily based NRMSEs are monthly aggregated and displayed in Table II.

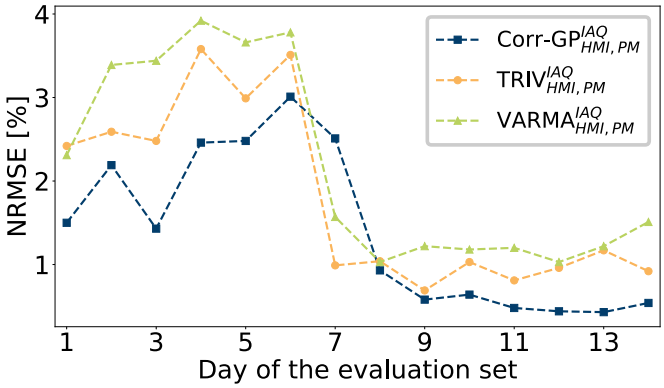

Fig. 4. Daily NRMSE-based comparison among the considered methods.

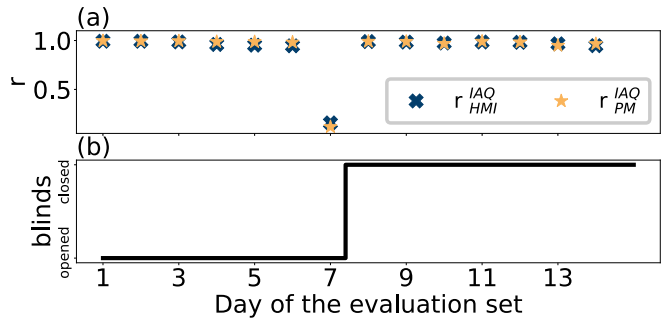

Fig. 5. (a) Pearson correlation coefficient of IAQ and HMI, PM measurements per day. (b) Blinds position.

TABLE II
NRMSE PER MONTH [%] OF LONG-TERM EVALUATION OF MULTIINPUT TEMPERATURE DT

	Jun	Jul	Aug	Sep	Oct	Nov	Dez
Corr-GP$^{IAQ}_{HMI,PM}$	1.3	2.2	3.3	3.8	6.3	7.3	6.4
TRIV$^{IAQ}_{HMI,PM}$	2.1	2.2	3.5	4.2	3.3	3.7	3.9
VARMA$^{IAQ}_{HMI,PM}$	2.0	2.1	3.5	4.0	3.1	3.5	3.8

It can be seen that the proposed Corr-GP$^{IAQ}_{HMI,PM}$ yields good results for the first months with consecutive increasing errors afterward. This can be rooted in seasonality effects and thus, a change in signal correlation. Consequently, for this type of model (15), dedicated retraining would be required, that is, additional measurements have to be performed limiting the usage of the DT model (15). It should be noted that although the performance of the trivial approach gets slightly worse over time, the NRMSE does not increase as much as the Corr-GP model. Before presenting a possible solution for the proposed Corr-GP approach in terms of the prior-mean function, we give more details on the individual signal's contribution in Section V-A3.

3) Model Selection, Limits, and Analysis of Corr-GP: To evaluate a possible model extension, consider single-input models first. In Fig. 6, the NRMSE of the continuous single-input models Corr-GP$^{IAQ}_{PM}$ and Corr-GP$^{IAQ}_{HMI}$ with zero prior-mean function, that is,

$$\mathcal{GP}\big(0, B_q^{[3]} \otimes K_{RQ}(\mathcal{T}, \mathcal{T}')\big), \tag{17}$$

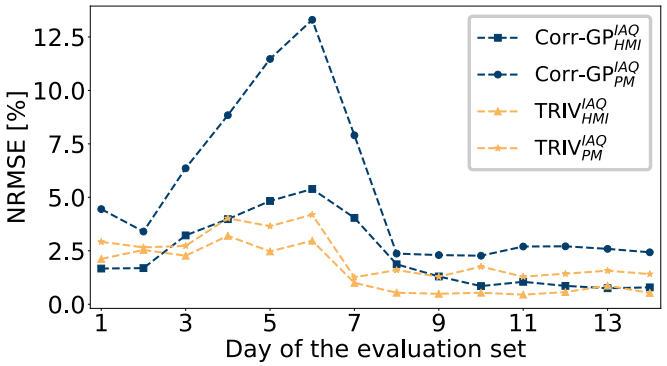

Fig. 6. NRMSE of single-input zero-mean Corr-GP and single-input TRIV.

with q = HMI or PM and TRIV$^{IAQ}_{PM}$ and TRIV$^{IAQ}_{HMI}$ are displayed. From Fig. 6, it can be deduced that the single-input GP architectures perform worse than the single-input trivial algorithm when evaluated for 14 days in June. In contrast, when having multiple measurement devices available, the results shown in Fig. 4 indicate that Corr-GPs are superior with a combination of several reference signals. This is because the correlations modeled by (8) are trainable hyperparameters of the proposed Corr-GP.

In addition to the NRMSE, intraday performance and individual outliers play a significant role in all follow-up processes based on pseudo-measurements, for example, building operations. More precisely, the intraday prediction accuracy and the correct estimation of the current system state directly affect the controller's ability to maximize individual TC and save energy. In Fig. 7, the normalized maximum deviation

$$\Delta T_{max} = \frac{1}{\bar{T}_{IAQ}} \max_{i=1,\dots,M_j} \{|T_{IAQ,i} - T_{DT,i}|\}, \tag{18}$$

is displayed in addition to the NRMSE. The max-operator determines the maximum deviation between the true T_{IAQ} and the predicted temperature T_{DT} for a single day normalized by the daily average $\bar{T}_{IAQ}$.

As can be seen in Fig. 7, a connection between NRMSE (blue) and ΔT_{max} (orange) is evident. More precisely, we can deduce that mostly if ΔT_{max} rises, so does the NRMSE. In other words, the performance of the proposed approach is primarily driven by short-term deviations. An example of this can be seen in Fig. 8, where two particular days are depicted.

Fig. 8(a) displays an example that gives a comparably high NRMSE of 2.46% and Fig. 8(b) shows a well-performing day with an NRMSE of 0.93%. In Fig. 8(a), it can be seen that the dynamics of the true IAQ measurements (blue crosses) clearly deviate from the two input reference sensors HMI (red) and PM (orange) after 4:30 pm. The local rise in temperature can be explained by an increase in the solar irradiation hitting the IAQ sensor but not the permanent ones. The filled gray area in Fig. 8 shows the measured indoor luminosity for the two days, indicating that: 1) high luminosity (i.e., solar irradiation) generally leads to high air temperatures and 2) solely the IAQ sensor reacts to the significant changes in measured luminosity. Due to a low solar elevation angle in the afternoon, the IAQ sensor, which is mounted at a lower height, is hit by incoming solar radiation increasing the measured temperature.

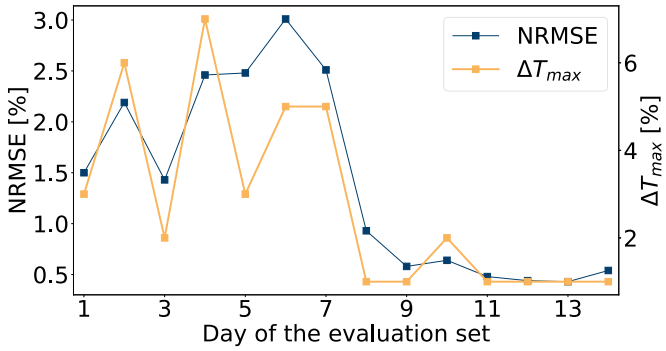

Fig. 7. Normalized maximum deviation $\Delta T_{\max}$ and NRMSE.

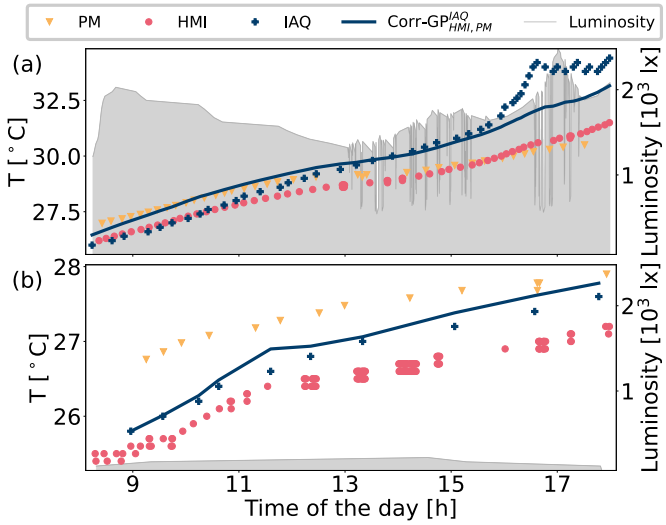

Fig. 8. Reference measurements, IAQ measurements, the predicted Corr-GP DT, and the luminosity for (a) day 4 and (b) day 8 are given.

However, the two permanent sensors which are mounted at higher heights are not exposed and, therefore, do not report a temperature increase. As this information is not provided to the DT Corr-GP$^{\text{IAQ}}_{\text{HMI,PM}}$ by the reference signals, it cannot be reproduced by the proposed approach.

B. Temperature Single-Input DT

Summarizing the discussion in Section V-A, the Corr-GP approach is superior to the given alternatives regarding the incorporation of multiple inputs but remains sensitive to broken correlations. In the remaining part of this work, we solve the latter issue as periodical retraining would limit the application in practical settings. As the incorporation of additional measurement signals is out of the scope of this work, we leave a dedicated analysis for future work.

The key observation from the previous discussion allowing us to extend the given approach is the good performance of the trivial alternative. More precisely, the trivial method TRIV can be included in the Corr-GP in terms of a prior mean function. It should be noted that in the given application it is not possible to give an analytic expression for the prior mean function. Thus, we propose

$$\text{DT}^{\text{IAQ}}_{\text{HMI}} = \mathcal{GP}\Big(\text{TRIV}^{\text{IAQ}}_{\text{HMI}}, B^{[2]}_{\text{HMI}} \otimes K_{\text{RQ}}(\mathcal{T}, \mathcal{T}')\Big). \tag{19}$$

The results for model (19) in terms of a long-term evaluation are displayed in Table III. It should be noted that only results

TABLE III
NRMSE PER MONTH [%] OF LONG-TERM EVALUATION OF THE SINGLE-INPUT TEMPERATURE DT

	Jun	Jul	Aug	Sep	Oct	Nov	Dez
Corr-GP$^{\text{IAQ}}_{\text{HMI}}$	1.2	1.1	3.0	3.7	3.0	2.4	2.5
TRIV$^{\text{IAQ}}_{\text{HMI}}$	1.7	2.0	3.3	4.2	3.2	3.1	3.1
VARMA$^{\text{IAQ}}_{\text{HMI}}$	1.8	1.8	3.1	4.0	3.1	3.1	3.2

for the model with HMI input are explicitly given due to better performance compared to the PM sensor as input.

In Table III, it can be seen that the proposed DT model (19) outperforms the given alternatives and provides a sufficient prediction capability. It should be noted that the independent accuracy of the proposed model regarding seasonalities is a result of the given analysis as no seasonal pattern can be observed for the results of Corr-GP$^{\text{IAQ}}_{\text{HMI}}$ in Table III. However, as discussed in Section III-C, this type of independence can be understood by construction. Contrary to the zero-mean approach (15) and (17), the proposed approach (19) is not trained on correlations across signals. Instead, it captures the deviations from an expected mean provided by the trivial approach. As seasonal changes affect all instances simultaneously, the proposed extension by Triv mean functions is also more resistant regarding changing seasonalities.

C. CO_2 DTs

For the second case study concerning CO_2 pseudo-measurements, both proposed models are tested and evaluated, while the single-input model is tested with both possible reference sensors PM and MS, individually. Summarizing the proposed approaches, we have

$$\text{DT}^{\text{IAQ}}_{\text{MS,PM}} = \mathcal{GP}\Big(0, \sum_{q=\text{MS,PM}} B^{[3]}_{q} \otimes K_{M^{5/2}}(\mathcal{T}, \mathcal{T}')\Big) \tag{20}$$

$$\text{DT}^{\text{IAQ}}_{\text{PM}} = \mathcal{GP}\Big(\text{TRIV}^{\text{IAQ}}_{\text{PM}}, B^{[2]}_{\text{PM}} \otimes K_{M^{5/2}}(\mathcal{T}, \mathcal{T}')\Big) \tag{21}$$

$$\text{DT}^{\text{IAQ}}_{\text{MS}} = \mathcal{GP}\Big(\text{TRIV}^{\text{IAQ}}_{\text{MS}}, B^{[2]}_{\text{MS}} \otimes K_{M^{5/2}}(\mathcal{T}, \mathcal{T}')\Big). \tag{22}$$

The results for both proposed approaches as well as the given alternatives are given in Table IV. From that, it can be seen that only the Corr-GP$^{\text{IAQ}}_{\text{MS}}$ outperforms the given alternative algorithms. As exemplarily shown in Fig. 9, this is rooted in the fact that the MS sensor yield measurements sufficiently correlated to the desired IAQ measurements. In contrast, the PM sensor displays a lower amount of correlation as evident from Fig. 9. Thus, both models including readings from PM display a worse performance.

D. Applications of Building DTs

We conclude this section with a comparison of the proposed approaches, discuss a practical implementation, and address limitations and future research directions.

1) Comparison: Regarding temperature pseudo-measurements, both proposed approaches outperform the given alternatives subjected to an unchanged seasonality. In the case of changing seasonality, the long-term results of Sections V-B and V-C indicate that the nonzero mean

TABLE IV
NRMSE PER MONTH [%] OF CO_2 DTS

		Jun	Jul	Aug	Sep	Oct	Nov	Dez
PM MS	Corr-$GP^{IAQ}_{MS,PM}$	8.1	6.8	13.7	11.3	12.4	13.1	14.2
	$TRIV^{IAQ}_{MS,PM}$	7.0	7.1	11.5	10.9	10.7	10.4	9.6
	$VARMA^{IAQ}_{MS,PM}$	7.0	6.9	11.2	13.8	11.9	8.3	12.3
PM	Corr-GP^{IAQ}_{PM}	10.1	12.9	22.9	23.7	24.4	24.4	23.1
	$TRIV^{IAQ}_{PM}$	8.8	10.7	21.0	21.9	22.7	22.7	21.5
	$VARMA^{IAQ}_{PM}$	8.3	9.6	20.0	20.9	21.6	21.8	20.6
MS	Corr-GP^{IAQ}_{MS}	6.9	6.3	5.6	5.5	5.2	4.9	4.7
	$TRIV^{IAQ}_{MS}$	7.7	7.6	6.3	6.9	6.1	5.8	5.9
	$VARMA^{IAQ}_{MS}$	7.9	7.7	6.5	7.1	6.3	6.0	6.0

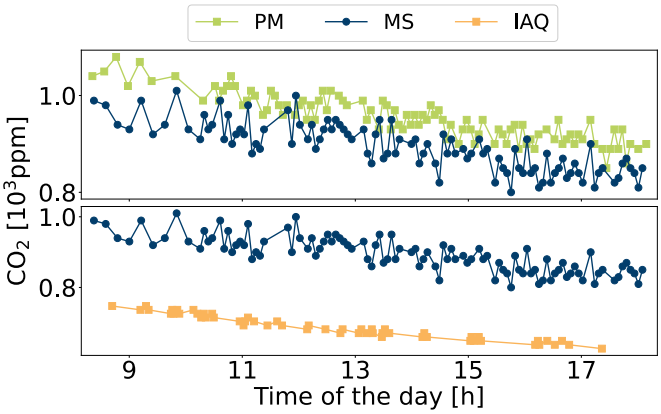

Fig. 9. Exemplary CO_2 data of a random day (Dec 2).

single-input model Corr-GP^{IAQ}_{MS} is applicable without retraining. Thus, long-term pseudo-measurements can be provided by Corr-GP^{IAQ}_{MS}. Comparison of Tables II and III shows a possible reduction from two reference sensors to one reference sensor if the GP approach with nonzero mean function Corr-GP^{IAQ}_{MS} is considered. With application to CO_2 pseudo-measurements, only the nonzero means single-input with the MS as a reference provides sufficient results.

Concerning the class of vector autoregressive approaches, like VARMA, it should be noted that they require nonseasonal data as they assume an underlying stationary stochastic process. As this is not the case for the given application, the data must be preprocessed to be usable by VARMA models. In the given case study, a trend-stationarity is not applicable as the test was aborted after ten evaluation days at most. This is due to a changing seasonal behavior during operation, which is not assignable by the training set. A common method is to consider the difference between neighboring data points. However, this is not applicable as there is no initial point to reverse this transformation to the actual signals. In contrast, the proposed Corr-GP approaches do not require any preprocessing.

In the given case study, small training datasets are considered. Although more data could be collected in principle, in practical applications, additional measurements should be limited to reduce hardware costs, implementation effort, and user disturbances to a minimum. In the presented case study

TABLE V
NUMBER OF AVAILABLE TRAINING DATA POINTS PER SENSOR

	Temperature			CO_2		
Sensor type	PM	HMI	IAQ	PM	MS	IAQ
# data points	155	462	197	377	543	562

with five training days, the number of available training data points is summarized in Table V. Thus, neural network architectures are not applicable due to the small amount of training data [30].

2) Implementation: The proposed approach is implemented in Python. A minimal set of preprocessing steps is applied, where the daytimes of each day are selected from the individual signals, and NaN values are filtered. The proposed approach is implemented using GPy [31]. For the given application, hyperparameter specifications are given by GPy's default settings. For the continuous update of the DT during offline operation, signals are retrieved from a database (CrateDB [32]).

The measurements obtained through the various sensors are collected and standardized at a PLC (cf. Table I). Via an edge-to-cloud adapter, based on PyADS [33] and the Eclipse Paho MQTT python client [34], and implemented in Python, we retrieve the standardized data from the PLC and forward it to an Eclipse Mosquitto MQTT broker [35]. From there, the data is written into the database via a script based on the CrateDB Python client library [36]. All scripts, the MQTT broker, and the database are deployed using Docker [37] in our self-hosted cloud environment built on OpenStack [38]. More details on the data collection infrastructure can be found in [28].

To apply the GP in an online manner, that is, for generating pseudo-measurements live, we, additionally, developed an MQTT interface that allows us to feed the GP directly with live data from the sensors.

3) Limits: A key aspect of the proposed approach is the sensitivity to correlations among signals. However, this might also be a limiting fact in practical application. For example, as described in Fig. 8, only one of the sensors might be affected by individual effects like shading. Turning the roles of the considered signals around, that is, using the IAQ as a reference sensor predicting HMI or PM in Fig. 8 would display a sensitive response to the single-sensor effect. Thus, care must be taken in sensor layout omitting single-sensor effects in reference sensors.

Depending on the type of included sensors and signals, sensor drifting can also not be neglected. As the proposed approach is trained on a specific correlation, retraining cannot be avoided in this case. Practically, this implies the installation of the sensor conducting training data, at which the pseudo-measurements should be performed. In general, retraining is always mandatory in cases, in which the correlations between the considered reference measurements and pseudo-measurements change.

In this work, we show that the proposed approach can be updated with respect to new, possibly sparsely sampled COV measurements. However, if the reference sensor fails to

provide any data, also the DT cannot be updated such that no pseudo-measurements can be provided.

4) Outlook: In future works, the demonstrated DTs could be applied to rooms and buildings having different characteristics. In particular, transfer learning could be investigated to reduce costs and implementation of additional measurement devices for training. It is expected that the benefits of the approach are larger in spaces where the distance and height between the remotely mounted sensors and the occupied zone are large, which could be examined as well.

As discussed in the last section, the prediction accuracy of the pseudo-measurements was demonstrated to be sensitive to various shading variables, like the position of the blinds and indoor illuminance. Adding such additional information by dedicated measurements could be used to feed the Corr-GP to improve the overall performance.

Although the proposed approach is trainable on small datasets which practically benefits a quick application omitting long periods of collecting training data, including data obtained during long-term application might be beneficial. In particular, the analysis of changes in a particular signal as well as across multiple reference signals might be used and could render retraining unnecessary.

VI. Conclusion

In this work, a DT architecture providing temperature and CO_2 pseudo-measurements realized by two types of Corr-GPs is proposed. In particular, a multiinput zero-mean as well as a single-input nonzero-mean Corr-GP is proposed and analyzed. It is shown that the proposed Corr-GP DT outperforms alternative approaches in predicting a close-to-person temperature and CO_2 pseudo-measurement based on remotely mounted measurement devices.

For temperature pseudo-measurements, both types of proposed Corr-GP DTs yield sufficient realizations in case of an unchanged seasonality. Moreover, for temperature pseudo-measurements, we show that in this case, Corr-GPs are of advantage when dealing with multiple reference measurements. Additionally, we provide results for single-input Corr-GP with a nonzero mean function, indicating a reliable long-term application. In particular, a dedicated retraining of the given DT can be avoided. For the CO_2 pseudo-measurements, only the single-input formulation yields sufficient results and outperforms the given alternatives.

References

[1] I. Khajehzadeh and B. Vale, "How new Zealanders distribute their daily time between home indoors, home outdoors and out of home," *Kōtuitui, New Zealand J. Social Sci. Online*, vol. 12, no. 1, pp. 17–31, Jan. 2017.

[2] European Union. (2022). *Eurostat Regional Yearbook: 2022 Edition*. [Online]. Available: https://data.europa.eu/doi/10.2785/915176

[3] L. Yang, H. Yan, and J. C. Lam, "Thermal comfort and building energy consumption implications—A review," *Appl. Energy*, vol. 115, pp. 164–173, Feb. 2014.

[4] Y. Geng, W. Ji, B. Lin, and Y. Zhu, "The impact of thermal environment on occupant IEQ perception and productivity," *Building Environ.*, vol. 121, pp. 158–167, Aug. 2017.

[5] *Ergonomics of the Thermal Environment—Analytical Determination and Interpretation of Thermal Comfort Using Calculation of the PMV and PPD Indices and Local Thermal Comfort Criteria*, Standard ISO 7730:2005, Int. Org. Standardization, Geneva, Switzerland, Nov. 2005.

[6] Y. Feng, S. Liu, J. Wang, J. Yang, Y.-L. Jao, and N. Wang, "Data-driven personal thermal comfort prediction: A literature review," *Renew. Sustain. Energy Rev.*, vol. 161, Jun. 2022, Art. no. 112357.

[7] S. C. Folea and G. D. Mois, "Lessons learned from the development of wireless environmental sensors," *IEEE Trans. Instrum. Meas.*, vol. 69, no. 6, pp. 3470–3480, Jun. 2020.

[8] S. Sun, H. Huang, T. Peng, and D. Wang, "An improved data privacy diagnostic framework for multiple machinery components data based on swarm learning algorithm," *IEEE Trans. Instrum. Meas.*, vol. 72, pp. 1–9, 2023.

[9] V. Scotti, "Big data or big (privacy) problem?" *IEEE Instrum. Meas. Mag.*, vol. 20, no. 5, pp. 23–26, Oct. 2017.

[10] A. Čulić, S. Nižetić, P. Šolić, T. Perković, and V. Čongradac, "Smart monitoring technologies for personal thermal comfort: A review," *J. Cleaner Prod.*, vol. 312, Aug. 2021, Art. no. 127685.

[11] A. K. Kanál and K. Tamás, "Assessment of indoor air quality of educational facilities using an IoT solution for a healthy learning environment," in *Proc. IEEE Int. Instrum. Meas. Technol. Conf. (I2MTC)*, May 2020, pp. 1–6.

[12] P. Althaus, F. Redder, E. Ubachukwu, M. Mork, A. Xhonneux, and D. Müller, "Enhancing building monitoring and control for district energy systems: Technology selection and installation within the living lab energy campus," *Appl. Sci.*, vol. 12, no. 7, p. 3305, Mar. 2022.

[13] V. A. Arowoiya, R. C. Moehler, and Y. Fang, "Digital twin technology for thermal comfort and energy efficiency in buildings: A state-of-the-art and future directions," *Energy Built Environ.*, vol. 5, no. 5, pp. 641–656, Oct. 2024.

[14] A. Fuller, Z. Fan, C. Day, and C. Barlow, "Digital twin: Enabling technologies, challenges and open research," *IEEE Access*, vol. 8, pp. 108952–108971, 2020.

[15] H. Zhao, Z. Zhang, Y. Yang, J. Xiao, and J. Chen, "A dynamic monitoring method of temperature distribution for cable joints based on thermal knowledge and conditional generative adversarial network," *IEEE Trans. Instrum. Meas.*, vol. 72, pp. 1–14, 2023.

[16] J. Kuprat, K. Debbadi, J. Schaumburg, M. Liserre, and M. Langwasser, "Thermal digital twin of power electronics modules for online thermal parameter identification," *IEEE J. Emerg. Sel. Topics Power Electron.*, vol. 12, no. 1, pp. 1020–1029, Feb. 2024.

[17] M. Yang et al., "Digital twin driven measurement in robotic flexible printed circuit assembly," *IEEE Trans. Instrum. Meas.*, vol. 72, pp. 1–12, 2023.

[18] M. Pau, F. Ponci, A. Monti, C. Muscas, and P. A. Pegoraro, "Distributed state estimation for multi-feeder distribution grids," *IEEE Open J. Instrum. Meas.*, vol. 1, pp. 1–12, 2022.

[19] H. Seo and W.-S. Yun, "Digital twin-based assessment framework for energy savings in university classroom lighting," *Buildings*, vol. 12, no. 5, p. 544, Apr. 2022.

[20] A. Schweigkofler et al., "Digital twin as energy management tool through IoT and BIM data integration," in *Proc. CLIMA Conf.*, Apr. 2022. [Online]. Available: https://proceedings.open.tudelft.nl/clima2022/article/view/46

[21] M. Vanin, T. Van Acker, R. D'hulst, and D. Van Hertem, "Exact modeling of non-Gaussian measurement uncertainty in distribution system state estimation," *IEEE Trans. Instrum. Meas.*, vol. 72, pp. 1–11, 2023.

[22] S. Lu, Y. Gong, H. Luo, F. Zhao, Z. Li, and J. Jiang, "Heterogeneous multi-task learning for multiple pseudo-measurement estimation to bridge GPS outages," *IEEE Trans. Instrum. Meas.*, vol. 70, pp. 1–16, 2021.

[23] M. Zimmer et al., "Building digital twins for thermal pseudo-measurements generation," in *Proc. IEEE Int. Instrum. Meas. Technol. Conf. (I2MTC)*, May 2024, pp. 1–6.

[24] S. Jain, Sanjay, Pawan, R. Arora, and P. Behera, "Wind power forecasting using VARMAX," in *Proc. 2nd Int. Conf. Technol. Adv. Comput. Sci. (ICTACS)*, Oct. 2022, pp. 353–360. [Online]. Available: https://ieeexplore.ieee.org/document/9988181

[25] C. Rasmussen and C. Williams, *Gaussian Processes for Machine Learning* (Adaptive Computation and Machine Learning). Cambridge, MA, USA: MIT Press, Jan. 2006.

[26] M. A. Alvarez, L. Rosasco, and N. D. Lawrence, "Kernels for vector-valued functions: A review," *Found. Trends Mach. Learn.*, vol. 4, no. 3, pp. 195–266, 2012.

[27] M. Mork, F. Redder, A. Xhonneux, and D. Müller, "Real-world implementation and evaluation of a model predictive control framework in an office space," *J. Building Eng.*, vol. 78, Nov. 2023, Art. no. 107619.
[28] F. Redder et al. (2024). *Information and Communication Technologies (ICT) for Holistic Building Energy System Operation in Living Labs: Conceptualization, Implementation, Evaluation*. [Online]. Available: https://ssrn.com/abstract=4743282
[29] X. Zhi, S. Yuexin, M. Jin, Z. Lujie, and D. Zijian, "Research on the Pearson correlation coefficient evaluation method of analog signal in the process of unit peak load regulation," in *Proc. 13th IEEE Int. Conf. Electron. Meas. Instrum. (ICEMI)*, Oct. 2017, pp. 522–527.
[30] A. Dairi, F. Harrou, S. Khadraoui, and Y. Sun, "Integrated multiple directed attention-based deep learning for improved air pollution forecasting," *IEEE Trans. Instrum. Meas.*, vol. 70, pp. 1–15, 2021.
[31] GPy. (2012). *GPy: A Gaussian Process Framework in Python*. [Online]. Available: http://github.com/SheffieldML/GPy
[32] Crate.io. (2013). *CrateDB: The Database for Real-Time Analytics and Hybrid Search*. [Online]. Available: https://cratedb.com/product/self-managed
[33] PyADS. (2015). *PyADS: A a Python Wrapper for TwinCATs ADS Library*. [Online]. Available: https://github.com/stlehmann/pyads
[34] Eclipse Foundation. (2014). *Eclipse Paho MQTT Python Client Library*. [Online]. Available: https://github.com/eclipse-paho/paho.mqtt.python
[35] (2009). *Eclipse Mosquitto: An Open Source MQTT Broker*. [Online]. Available: https://mosquitto.org/
[36] Crate.io. (2013). *Python DB API Client Library for CrateDB, Using HTTP*. [Online]. Available: https://github.com/crate/crate-python
[37] Docker. (2013). *Docker: Develop Faster. Run Anywhere*. [Online]. Available: https://www.docker.com/
[38] Open Infrastructure Foundation. (2010). *OpenStack: The Most Widely Deployed Open Source Cloud Software in the World*. [Online]. Available: https://www.openstack.org/

Marcel Zimmer received the B.Sc. and M.Sc. degrees in physics from the University of Cologne, Cologne, Germany, in 2014 and 2018, and the B.Sc. degree in mathematics from the University of Cologne, in 2018. Currently, he is pursuing the Ph.D. degree with the Institute of Climate and Energy Systems (ICE-1), Research Center Jülich, Jülich, Germany.

Maximilian Buechel received the B.Sc. and M.Sc. degrees in physics from Dortmund University of Technology, Dortmund, Germany, in 2021 and 2024, respectively. Currently, he is pursuing the Ph.D. degree with the Institute of Climate and Energy Systems (ICE-1), Research Center Jülich, Jülich, Germany.

Florian Redder received the B.Sc. degree in mechanical engineering and the M.Sc. degree in energy engineering from RWTH Aachen University, Aachen, Germany, in 2016 and 2018, respectively. Currently, he is pursuing the Ph.D. degree with the Institute of Climate and Energy Systems (ICE-1), Research Center Jülich, Jülich, Germany.

Maximilian Mork received the B.Sc. degree in mechanical engineering, the M.Sc. degree in energy engineering, and the Ph.D. degree from RWTH Aachen University, Aachen, Germany, in 2015, 2017, and 2024, respectively.

Currently, he is working as a Research Assistant with the Institute of Climate and Energy Systems (ICE-1), Research Center Jülich, Jülich, Germany.

Thiemo Pesch received the Diploma degree in electrical engineering and information technology as well as in economic studies and the Ph.D. degree from RWTH Aachen University, Aachen, Germany, in 2009 and 2019, respectively.

Currently, he is the Head of the Departments "Energy Grids" and "High Performance Computing," Institute of Climate and Energy Systems (ICE-1), Research Center Jülich, Jülich, Germany.

André Xhonneux received the Diploma and Ph.D. degrees in mechanical engineering from RWTH Aachen University, Aachen, Germany, in 2008 and 2015, respectively.

Currently, he is the Department Leader of the "Buildings and Districts" group at the "Institute of Climate and Energy Systems: Energy Systems Engineering, ICE-1," Forschungszentrum Jülich, Jülich, Germany.

Dirk Müller received the B.Sc. degree from Thayer School of Engineering at Dartmouth, Hanover, NH, USA, in 1994, and the Diploma and Dr.-Ing. degrees in mechanical engineering from RWTH Aachen University, Aachen, Germany, in 1995 and 1999, respectively.

From 2003 to 2007, he was a Full Professor (W4) and the Director of the Hermann-Rietschel Institute, Technical University of Berlin, Berlin, Germany. Currently, he is the Director of the "Institute of Climate and Energy Systems: Energy Systems Engineering, ICE-1," Forschungszentrum Jülich (since 2017), Jülich, Germany, and a Full Professor (W3) and the Director of the Institute of Institute for Energy Efficient Buildings and Indoor Climate at E.ON Energy Research Center, RWTH Aachen University (since 2007).

Andrea Benigni (Senior Member, IEEE) received the B.Sc. and M.Sc. degrees from Politecnico di Milan, Milan, Italy, in 2005 and 2008, respectively, and the Ph.D. degree from RWTH Aachen University, Aachen, Germany, in 2013.

From 2014 to 2019, he was an Assistant Professor with the Department of Electrical Engineering, University of South Carolina, Columbia, SC, USA. Since 2019, he has been a Full Professor with RWTH Aachen University and the Director of the "Institute of Climate and Energy Systems: Energy Systems Engineering, ICE-1," Forschungszentrum Jülich, Jülich, Germany.